# Engineering the mechanical and physical properties of organic–inorganic composite microcapsules

Long, Yue; Song, Kai; York, David; Zhang, Zhibing; Preece, Jon A.

*DOI:*
10.1016/j.colsurfa.2013.04.055



*Document Version*
Publisher's PDF, also known as Version of record

*Citation for published version (Harvard):*
Long, Y, Song, K, York, D, Zhang, Z & Preece, JA 2013, 'Engineering the mechanical and physical properties of organic–inorganic composite microcapsules', *Colloids and Surfaces A: Physicochemical and Engineering Aspects*, vol. 433, pp. 30-36. https://doi.org/10.1016/j.colsurfa.2013.04.055

Colloids and Surfaces A: Physicochem. Eng. Aspects 433 (2013) 30–36

Contents lists available at SciVerse ScienceDirect

Colloids and Surfaces A: Physicochemical and Engineering Aspects

journal homepage: www.elsevier.com/locate/colsurfa

# Engineering the mechanical and physical properties of organic–inorganic composite microcapsules

Yue Long[a,b,*,1], Kai Song[b], David York[c], Zhibing Zhang[d], Jon A. Preece[a,*]

[a] School of Chemistry, University of Birmingham, Edgbaston, Birmingham, B15 2TT, UK
[b] Beijing National Laboratory for Molecular Sciences, Institute of Chemistry, Chinese Academy of Sciences, Zhongguancun North First Street 2, Beijing, 100190, China
[c] Institute of Particle Science & Engineering, School of Process, Environmental and Materials Engineering, University of Leeds, Leeds, LS2 9J, UK
[d] School of Chemical Engineering, University of Birmingham, Edgbaston, Birmingham, B15 2TT, UK

## HIGHLIGHTS

- Double-shell composite microcapsules were synthesized.
- Mechanical property and leakiness of the microcapsules were characterized.
- SEM, TEM, GC and micromanipulation techniques were employed.
- The strength and leakiness of the microcapsules could be engineered separately.

## GRAPHICAL ABSTRACT

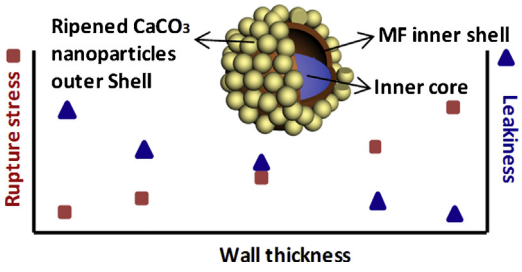


## ARTICLE INFO

*Article history:*
Received 4 March 2013
Received in revised form 19 April 2013
Accepted 28 April 2013
Available online 6 May 2013

*Keywords:*
Microcapsule
Pickering emulsion
Composite
Double-shell
Controlled delivery

## ABSTRACT

Double-shell composite microcapsule with a ripened $CaCO_3$ nanoparticle outer shell and melamine formaldehyde (MF)/copolymer inner shell shows advantages in adjustable permeability and mechanical strength, comparing with single shell microcapsules. Here, we have systematically studied the effects of certain formulation parameters on the properties of the double-shell composite microcapsules, i.e. the MF cross-linking time and the concentration of the aqueous $CaCl_2$ and $Na_2CO_3$ used for the ripening process of $CaCO_3$ nanoparticles. The properties of the microcapsules such as average diameter, wall thickness, degree of wall formation formed by the ripened $CaCO_3$ nanoparticles, nominal rupture stress and leakiness were characterized.



## 1. Introduction

Calcium carbonate is a natural shell material. It is non-toxic, stable, biocompatible and strong [1]. Therefore, in nature it is able to act as a physical barrier in shells to protect organisms from the environment, while allowing the gas and nutrient exchange through the shell. Biomimetic core–shell structured microcapsules have been developed to encapsulate active ingredients to protect them from an external environment [2–4]. Recently, calcium carbonate has attracted considerable attention for making walls of microcapsules due to its biocompatibility and pH triggered release mechanism [5,6]. Thomas et al. [7] have utilised a membrane technique to prepare $CaCO_3$ microcapsules, creating a pseudo water-in-oil-in-water emulsion system to precipitate calcium carbonate at the oil–water interface. The preparation of hollow $CaCO_3$

* Corresponding authors at: School of Chemistry, University of Birmingham, Edgbaston, Birmingham, B15 2TT, UK. Tel.: +44 0121 414 3528.
*E-mail addresses:* longyue@iccas.ac.cn (Y. Long), j.a.preece@bham.ac.uk (J.A. Preece).
[1] Tel.: +86 10 82617303.

0927-7757/$ – see front matter © 2013 Elsevier B.V. All rights reserved.
http://dx.doi.org/10.1016/j.colsurfa.2013.04.055

**Table 1**
Microcapsules batches **1**–**6**.

| Batch no. | Reaction time (h) | Concentration of $CaCl_2$ (aq) and $Na_2CO_3$ (aq) (M) |
|---|---|---|
| **1** | 4 | 1.5 |
| **2** | 8 | 1.5 |
| **3** | 4 | 0 |
| **4** | 24 | 1.0 |
| **5** | 24 | 1.5 |
| **6** | 24 | 2.0 |

microspheres is also an active field [8–10]. Such $CaCO_3$ microcapsules and microspheres have been used in a variety of industrial products, especially in biological applications [11–13]. However, the calcium carbonate wall possesses greater porosity when compared to organic wall materials [14,15], which limits its applications in encapsulation of small molecules.

We have previously introduced a methodology of forming double-shell composite microcapsule with a ripened $CaCO_3$ nanoparticle outer shell and melamine formaldehyde (MF)/copolymer inner shell to reduce the permeability [16]. As the mechanical properties and leakiness are two essential parameters of microcapsules in many applications. For different uses the mechanical strength and leakiness of microcapsules are always needed to be increased or decreased in order to meet the specific demands. In this paper, we made a systematic study of the effect of $CaCO_3$ nanoparticulate ripening process and MF cross-linking reaction time on the following physical properties of the microcapsules: wall thickness and completeness, nominal rupture stress and leakage of core oil, in order to manipulate the mechanical strength and leakiness of the microcapsules accordingly.

## 2. Materials and methods

### 2.1. Materials

The core oil is a typical organic blend of various fragrant components which has a relatively low solubility in water and is used in consumer products. MF precondensate (70% (aq), w/w, formaldehyde to melamine molar ratio 0.20) was supplied by British Industrial Plastics Ltd., Birmingham, UK, formaldehyde (37% (aq), w/w) was supplied by Sigma–Aldrich, UK. Poly(acrylamide–acrylic acid, sodium salt) was supplied by Polymersciences, Inc., US and $CaCO_3$ nanoparticles were supplied by Omya, UK. All chemicals were used without further purification.

### 2.2. Preparation of ripened double shell composite microcapsules

An aqueous solution of MF precondensate (2.50 g) and copolymer (0.58 g, poly(acrylamide–acrylic acid, sodium salt) in water (70 mL) was stirred (400 rpm) with a Rushton turbine (31 mm, in a vessel with standard configuration) for 105 min at pH 4 (adjusted by acetic acid (1 M), monitored by a pH meter) to form pre-crosslinked MF precondensate and copolymer. The core oil (9.3 g) was added to an aqueous $CaCO_3$ nanoparticle dispersion (40 mL, 10% wt) and stirred using a homogenizer (Silverson Machines Ltd.) at a speed of 2500 rpm for 3 min to form an o/w emulsion. To the resulting emulsion, aqueous $CaCl_2$ (10 mL) and $Na_2CO_3$ (10 mL) (1.0, 1.5 and 2.0 M for **batches 4**, **5** and **6** (Table 1), respectively) was added via a pump system (Model 101U, Water Marlow, UK) over 15 min, and stirred for another 10 min at a speed of 400 rpm. To the resulting aqueous dispersion, the pre-crosslinked MF precondensate and copolymer solution was then added via a pump system (Model 101U, Water Marlow, UK) over 10 min, and the pH was raised to 6.0 with the addition of aqueous NaOH (1 M, monitored by a pH meter). The resulting dispersion was stirred at a speed of 400 rpm at 65 °C for 4, 8, and 24 hours for batches **1** and **3**, **2**, and **4**–**6**, respectively, and was allowed to cool to room temperature. The exact conditions for producing the double shell composite microcapsules batches **1**–**6** are listed in Table 1.

### 2.3. Environmental scanning electron microscopy (ESEM)

Environmental-SEM (FEI/Philips XL30 ESEM-FEG, Philips, UK) with an operating voltage shown in images was used to study the morphology of the microcapsules. Samples were operated in high vacuum mode.

### 2.4. Transmission electron microscopy (TEM)

Transmission Electron Microscopy (JEOL 1200EX, Jeol Ltd., UK) operating at 80 eV was used to examine the structure and thickness of the microcapsule wall. Microcapsules were embedded in LR white hard grade acrylic resin, and the ultra thin sections (90–150 nm) were obtained by using an ultracut microtome (Reichert-Jung), see below.

#### 2.4.1. Sampling by ultra-microtome

The microcapsule dispersions (2 mL) were centrifuged at a speed of 500 rpm for 3 min, and the supernatant liquid was separated. Gluteraldehyde (2 mL) was added and the microcapsules were re-dispersed by gently shaking the vial manually. The resulting microcapsule dispersions were stored for 1 h to harden the outer shell of the microcapsules by cross-linking the microcapsule wall with gluteraldehyde, and centrifuged for 3 min at 500 rpm. The supernatant liquid (excess gluteraldehyde) was separated, and a solution of ethanol and water was added (1:1 volume ratio, 2 mL in total), and shaken by hand. The resulting mixture was centrifuged again at 500 rpm for 15 min, and the supernatant ethanol/water mixture was separated. The ethanol/water process was repeated four times, but with ethanol/water of 70:30, 90:10, 96:4 (volume), and finally the microcapsules were suspended in absolute ethanol. The resulting microcapsules dispersion was centrifuged again at 500 rpm for 15 min, and the supernatant liquid (excess absolute ethanol) was decanted. To the microcapsule slurry was added absolute ethanol and LR white resin (1:1, 2 mL), and the microcapsules were re-dispersed by gently shaking the vial manually. The resulting mixture was put on a rotator at a speed of 4 rpm. After ~3 min the microcapsules were displaced to the bottom of the vial, and rotating continued for a total of 3 h. The supernatant ethanol/resin solution was separated. 100% of LR white resin (2 mL) was added to the resulting microcapsule slurry, before they were rotated again at 4 rpm for 12 h, and the microcapsules were separated from the supernatant. Two beam capsules (15 mm × 5 mm) were filled to the top with the air free LR white resin (2 mL). The separated microcapsules were added to each resin filled beam capsule. The microcapsules settled on the bottom of the beam capsules. The mixture was heated (60 °C) under vacuum for 30 min, then left to cure for 48 h at 60 °C, affording a polymerized resin-microcapsule block. The resulting block was secured into a REICHERT-JUNG ultramicrotome apparatus and the microcapsule end was trimmed to sections of thickness 90–150 nm. The gold coloured sections were placed on carbon coated grids (G2500 C, 2 mm × 1 mm slot, copper, 3.05 mm) ready to be examined by TEM. The wall thicknesses of microcapsules were measured from the analysis of their TEM images of the ultra microtome sections.

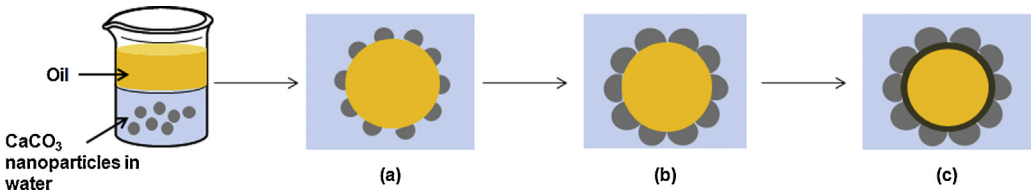


**Scheme 1.** Schematic diagram of the formation of the double-shell composite microcapsules. (a) o/w Emulsion stabilized by $CaCO_3$ nanoparticles was formed by emulsifying core oil and aqueous dispersion of $CaCO_3$ nanoparticles. (b) Addition of aqueous $CaCl_2$ and $Na_2CO_3$ (1.0/1.5/2.0 M) into (a) to form the ripened o/w emulsion stabilized by $CaCO_3$ nanoparticles. (c) Ripened double-shell composite microcapsules were formed by the addition of pre-crosslinked MF and copolymer into (b), and heated at 65 °C for 4/8/24 h.

### 2.5. Calculation of the wall thickness and degree of wall completeness of the ripened $CaCO_3$ nanoparticles from TEM images

The wall thickness for each microcapsule was obtained by measuring 30 different parts of the microcapsule wall from the TEM image, and taking the average value. For each batch, 30 microcapsules were measured. The degree of completeness of the ripened $CaCO_3$ nanoparticles of the double-shell composite microcapsules was calculated from an image analysis software (Image J, National Institutes of Health, USA) on the ultra microtome TEM images, by using the sum of the smallest perpendicular distance between each disconnected piece of the wall, subtracting this value from the total wall perimeter, and dividing by the total wall perimeter. For each batch, 30 microcapsules were measured.

### 2.6. Leakiness measurement

The microcapsules were filtered from the original aqueous dispersion, and re-dispersed in deionized water (50 mL). To the resulting aqueous dispersion (**batches 1–6**), hexane (30 mL) was added and stirred for 10 min and then stopped. A hexane aliquot (1 μL) was removed and analysed by gas chromatography (GC). Further aliquots (1 μL) were removed at various time intervals between 1 and 24 h, prior to which the dispersion was stirred for 10 min.

### 2.7. Size analysis

Mean particle size and size distribution of the microcapsules in aqueous dispersions were evaluated by a laser diffraction technique (Mastersizer 2000, Malvern Instruments Ltd., UK). The measurements were carried out using a Helium–Neon laser with a measurement range of 0.05–900 μm connected to a sample dispersion unit. Experiments were performed at 25 °C. The mean diameter and size distribution of microcapsules were the average value of five measurements.

### 2.8. Micromanipulation

The mechanical properties of the microcapsules were determined by micromanipulation. A glass probe with a diameter of 50 μm mounted on a force transducer (Model 405A, Aurora Scientific Inc., Canada) was positioned perpendicular to the glass slide. The microcapsules in aqueous dispersions were dried on the glass slide, and observed through side and bottom-view cameras. A single microcapsule was compressed by the glass probe travelling at 2 μm $s^{-1}$. The voltage output generated by the transducer due to compression of the microcapsule was recorded through a data acquisition card in a personal computer. From the sensitivity of the transducer, the voltage was converted to force; hence the rupture force of the microcapsule was determined. Details of this technique are described elsewhere [17].

## 3. Results and discussion

### 3.1. Synthesis

The double-shell composite microcapsules were prepared using a method based on in situ polymerization of MF with a copolymer migrating though the interstice of the ripened $CaCO_3$ shell, and polymerizing at the oil–water interface inside the ripened $CaCO_3$ nanoparticulate shell. The synthesis is illustrated in Scheme 1. Core oil was mixed with the aqueous $CaCO_3$ nanoparticulate dispersion to form the o/w emulsion followed by the addition of equivalent amount of aqueous $CaCl_2$ and $Na_2CO_3$ (1.0, 1.5 and 2.0 M, respectively) to ripen the $CaCO_3$ nanoparticles. Finally, the pre-crosslinked MF precondensate and copolymer formed by mixing the MF precondensate and copolymer (poly(acrylamide–acrylic acid, sodium salt)) in water for 105 min at pH 4.3 were added to the resulting ripened $CaCO_3$ nanoparticulate aqueous dispersion, which was heated at 65 °C for 4, 8 and 24 h, respectively. **Batches 1–6** were prepared as detailed in Table 1.

### 3.2. Wall thickness and degree of wall completeness

The wall thickness and degree of wall completeness formed by the $CaCO_3$ nanoparticles for **batches 1–6** microcapsules were evaluated and studied from the TEM images of the ultra-microtome sections, as shown in Fig. 1. As one might expect neither the outer $CaCO_3$ wall thickness of the double-shell composite microcapsules (402 ± 36, 406 ± 41 and 410 ± 47 nm for **batches 1**, **2** and **5**, respectively (Fig. 2)) nor the degree of wall formation formed by the ripened $CaCO_3$ nanoparticles (92.9 ± 0.5%, 93.0 ± 0.5% and 93.3 ± 0.4% for **batches 1**, **2** and **5**, respectively) is significantly affected by the MF cross-linking reaction time. However, during the ultra-microtome sampling, some parts of the MF polymer inner wall were detached from the outer $CaCO_3$ nanoparticluate wall. The detachment allowed us to measure the MF wall thickness as a function of reaction time. The wall thickness of the MF polymer increased from 129 ± 2.5 nm **(batch 1**, 4 h) to 160 ± 3.1 nm (**batch 5**, 24 h) when the MF cross-linking time increased from 4 to 24 h. Previous studies on the kinetics of the MF polymerization reaction showed that the polymerization mainly took place during the first 2–3 h of the reaction [18,19], which is in agreement with our result that the wall thickness does not increase much as the cross-linking time increased from 4 to 24 h. Prolonged reaction time produces more cross-linked network, and consequently results smaller pores on the wall [20].

A significant increase in the $CaCO_3$ wall thickness from 360 ± 41 nm (**batch 4**) to 580 ± 48 nm (**batch 6**) was observed when the concentration of aqueous $CaCl_2$ and $Na_2CO_3$ increased from 1.0 to 2.0 M (Fig. 2). However, the degree of wall formation formed by the ripened $CaCO_3$ nanoparticles remained unchanged (**batch 4–6**, ~93%), so did the inner MF/copolymer wall thickness (**batch 4–6**, ~160 nm). In addition, by ripening the $CaCO_3$ nanoparticulate wall, the $CaCO_3$ wall thickness increased from

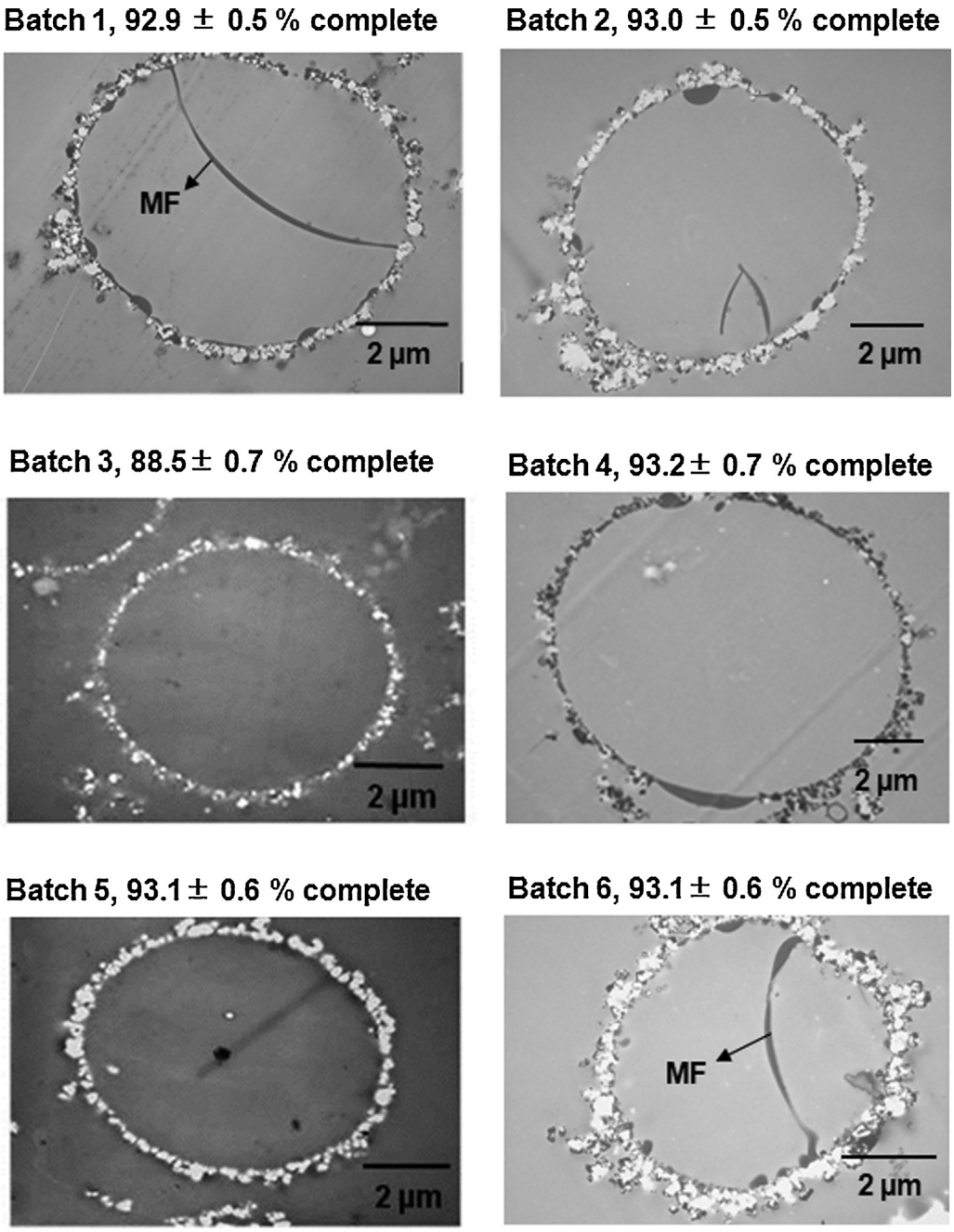


**Fig. 1.** Wall thicknesses and the degree of wall completeness of the ripened double-shell composite microcapsules batches **1**–**6**.

210 ± 21 (**batch 3**, 0 M) nm to 402 ± 36 nm (**batch 1**, 1.5 M), and the degree of wall completeness increased from 88.5 ± 0.7% to 92.9 ± 0.5%. This increase from **batch 3** to **batch 1** is as expected due to the $CaCO_3$ ripening process, that the aqueous $CaCl_2$ and $Na_2CO_3$ formed $CaCO_3$ fills the gaps between the original $CaCO_3$ nanoparticulates outer shell. Analysis of Fig. 1 **batches 4**, **5** and **6** in which increasing the concentration of $CaCl_2$ and $Na_2CO_3$ were added during the ripening process, leads us to propose the growth mechanism of the nanoparticulate $CaCO_3$ wall as follows. There are three ways in which the wall could ripen. We can imagine that the $CaCl_2$ and $Na_2CO_3$ solution nucleate growth on the surface of the $CaCO_3$ nanoparticles, or the $CaCl_2$ and $Na_2CO_3$ forming particulates in the solution and depositing on the nanoparticulate $CaCO_3$ wall. Also, the $CaCO_3$ ripening process could happen as a combination of both two types. In this study, revealed by the TEM images (Fig. 1), the $CaCO_3$ wall ripening process is more likely to be the combination of both $CaCO_3$ particle growth and deposition.

### 3.3. Average diameter and distribution

The average diameter and distribution of batches 1–6 are measured by laser diffraction and the results are graphically presented in Fig. 3. It shows that the average diameters for **batches 1**–**6** are ~14 μm. All 6 batches show bimodal distributions centered on 1–2 μm and 13–15 μm. The first peak (centered on 1–2 μm) is probably due to small melamine formaldehyde particulates formed at elevated temperature during the MF cross-linking process [21,22] combined with the solid $CaCO_3$ nanoparticles that were not contributing to the wall formation process. As we know that in a pickering emulsion system, the diameter is mainly determined by

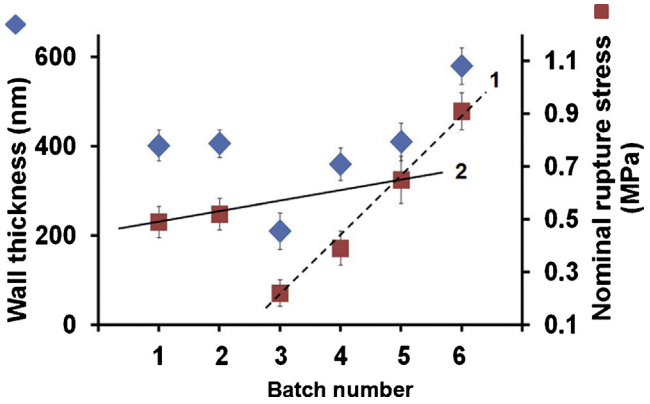


**Fig. 2.** $CaCO_3$ Wall thickness and nominal rupture stress for the ripened double-shell composite microcapsules batches **1**–**6**.

the emulsifying speed, oil/water ratio, and the amount of particles used in the emulsification stage. This is in agreement with our result that neither the MF cross-linking time nor the $CaCO_3$ wall thickness affects the stability of the initial droplet formed during the emulsification step. Hence, the average diameter and size distribution are not changed.

### 3.4. Mechanical properties

The mechanical properties of **batches 1**–**6** are evaluated using the micromanipulation technique. A typical relationship of the force imposed on a single microcapsule as a function of the probe moving distance is shown in Fig. 4 for a batch **1** microcapsule. After point **I** the probe touches the microcapsule, and the force imposed on the microcapsule increases until point **II** at which the microcapsule ruptures. As a result, the force drops to point **III**. The probe continues to compress the debris of the microcapsule (**III**–**IV**) until it touches the slide at point **IV**, after which the force increases as the probe pushes onto the slide. From this curve, the rupture force of the microcapsule can be determined (point **II**). The displacement at rupture ($\delta_R$) is denoted as the distance that the probe travels from contact with microcapsule until rupture. The deformation at rupture is calculated using Eq. (1) ($d$ = initial microcapsule diameter), and the nominal rupture stress is calculated using Eq. (2) as shown below, where $F_R$ is the rupture force (point **II**).

$$\text{Deformation at rupture } (\%) = \frac{\delta_R}{d} \times 100 \quad (1)$$

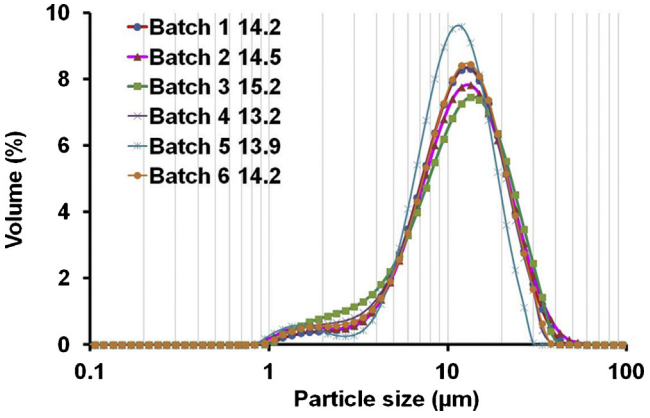


**Fig. 3.** Average diameter and size distribution of the ripened double shell composite microcapsules batches **1**–**6**.

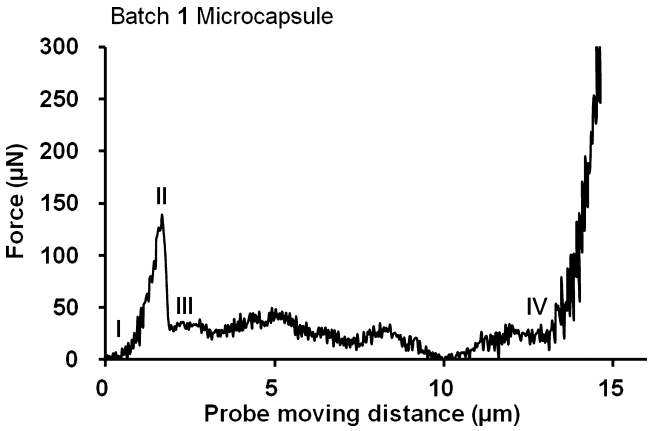


**Fig. 4.** Typical force vs. probe moving distance curve obtained by compressing one of the microcapsules in **batch 1**; I: probe/microcapsule contact, I–II: microcapsule compression, II: microcapsule ruptured, III-IV: probe compressing the broken debris, IV: probe touching the glass slide.

$$\text{Norminal rupture stress} = \frac{F_R}{\pi(d/2)^2} \quad (2)$$

The nominal rupture stress and wall thickness for all the 6 batches are presented in Fig. 2. The deformation at rupture for all 6 batches are indeterminate of altering the $CaCO_3$ nanoparticulate ripening process or the MF cross-linking reaction time, as all microcapsules deformed by ~7.5% at rupture. However, the nominal rupture stress increased from $0.22 \pm 0.05$ (**Batch 4**) to $0.91 \pm 0.07$ MPa (**Batch 6**, Fig. 2) when the concentration of $CaCl_2$ and $Na_2CO_3$ increased in the $CaCO_3$ nanoparticulate ripening process (**line 1**). Also, we can see that the increase in nominal rupture stress follows closely the increase in wall thickness of the $CaCO_3$ outer wall. There is a slight increase of nominal rupture stress from $0.49 \pm 0.06$ to $0.65 \pm 0.09$ when MF cross-linking time increased (**line 2**). However, when taking errors into consideration, we cannot safely conclude that prolonged cross-linking of MF enhanced the nominal rupture stress of the microcapsules. Hence, we propose that the rupture stress is dominantly contributed by the inorganic $CaCO_3$ outer shell [16]. The displacement at rupture, rupture force and nominal stress at rupture as a function of diameter for batch **6** microcapsules are plotted, and are shown in Fig. 5a–c, respectively. It was observed that for the same type of microcapsules, the displacement at rupture (Fig. 5a) and rupture force (Fig. 5b) increase as the diameter of the microcapsules increases. In contrast, the nominal stress at rupture (Fig. 5c) decreases as the particle diameter increases. The stress at rupture of the microcapsules may be directly related to their rupture behaviour in processing equipment. Larger microcapsules were found to rupture more easily than smaller ones in the previous studies [23]. Similar trends are also seen in microcapsules **1**–**6** (Please find the micromanipulation data for **batches 1**–**6** in the supporting information **S1**, **S2** and **S3**).

### 3.5. Leakiness

The leakiness of the **1**–**6** microcapsules was monitored over a period of 24 h and the results are plotted in Fig. 6. It can be seen that the unripened double-shell microcapsules (**Batch 3**) has a much larger leakiness ($0.15 \pm 0.011\%$) after 24 h in comparison with the ripened double-shell microcapsules ($0.047 \pm 0.002\%$) (**Batch 1**). However, when the concentration of the aqueous $CaCl_2$ and $Na_2CO_3$ in the ripening process increased from 1.0 to 2.0 M, the leakiness of the microcapsules only decreased from $0.052 \pm 0.001\%$ (**batch 4**) to $0.045 \pm 0.001\%$ (**batch 6**). We found this leakiness result correlates well with the wall structure, that the higher leakiness of the unripened microcapsules might be resulted from their lower

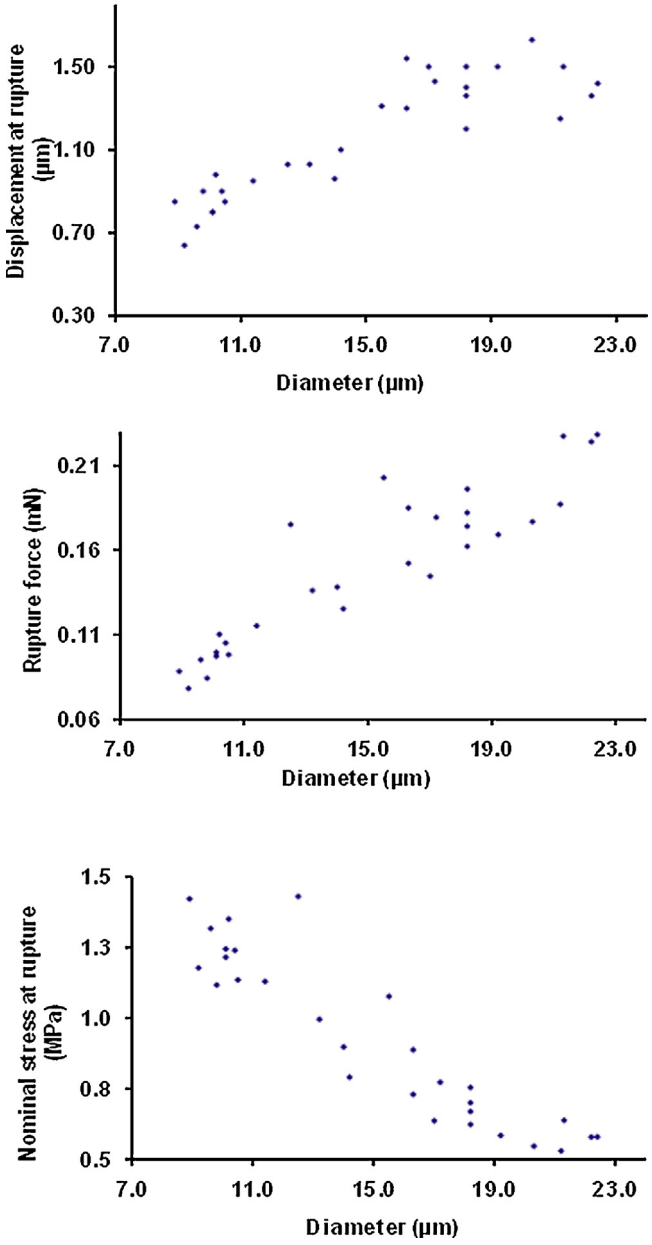


**Fig. 5.** Displacement at rupture vs. diameter, rupture force vs. diameter, and nominal stress at rupture vs. diameter for the ripened double shell composite microcapsules **batch 6**.

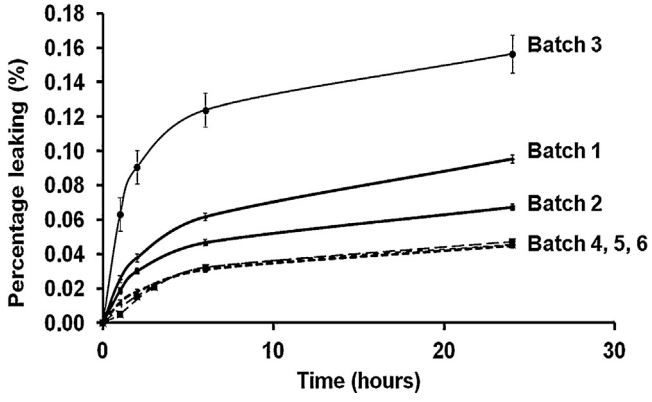


**Fig. 6.** Leakiness of the ripened double shell composite microcapsules **batches 1–6**.

degree of completerness of the wall compare to the ripened ones. The less reduction in leakiness between the ripened microcapsules **batch 4–6** might be due to their very similar completeness of wall (~93%). Nevertheless, when the MF cross-linking reaction time is increased from 4 (**batch 1**) to 24 (**batch 5**) hours, the leakage of the ripened double-shell composite microcapsules decreased (from $0.095 \pm 0.002\%$ to $0.047 \pm 0.001\%$). This decrease in leakage is probably due to the formation of a thicker and more compact MF polymer wall (Fig. 1, **batch 1** and **5**) resulting from the longer cross-linking reaction time. The leakage behaviour indicates that increasing the organic MF/copolymer inner wall thickness and compactness is a more effective way for preventing the oil leakage than further increasing the thickness of $CaCO_3$ outer shell.

## 4. Conclusion

We have successfully prepared ripened double-shell composite microcapsules with an organic MF/copolymer inner shell and an inorganic ripened $CaCO_3$ nanoparticulate outer shell. It was found that by ripening the $CaCO_3$ outer shell, the completeness of the microcapsules wall increased, the nominal rupture stress increased, and consequently the leakiness of the microcapsules was reduced. Hence, ripening process is a significant step for improving the mechanical and physical stabilities of the double-shell composite microcapsules. As we further adjust the concentration of the aqueous $CaCl_2$ and $Na_2CO_3$ in the ripening step to modulate the wall thickness of the $CaCO_3$ outer shell. We found that when the $CaCO_3$ wall thickness increased, the nominal rupture stress increased, the leakiness remained unchanged. In contrast, the concentration of the aqueous $CaCl_2$ and $Na_2CO_3$ increased leading to the $CaCO_3$ nanoparticulate ripening process, both the ripened $CaCO_3$ wall thickness of the microcapsules and the nominal rupture stress of the microcapsules increased, and the leakiness of the microcapsules decreased. When increasing the MF polymerization time, the MF/copolymer inner wall thickness increased, resulting in the decrease of the leakiness of the microcapsules. Therefore, we conclude that the mechanical properties of the double-shell composite microcapsules were dominated by the $CaCO_3$ outer shell, whereas the leakage of the microcapsules was primarily governed by the MF inner shell. Thus, we now have a process whereby we can engineer the strength of the microcapsules independently of the leakiness.

## Acknowledgements

Yue Long was supported by the School of Chemistry, University of Birmingham through Overseas Research Student Awards Scheme funding, Procter and Gamble and Advantage West Midland (AWM) and the European Research Development Fund (ERDF) through Science City, Advanced Materials Project 2 (Innovative Uses for Advanced Materials in the Modern World), and the EPSRC (EP/F068395/1).

## Appendix A. Supplementary data

Supplementary data associated with this article can be found, in the online version, at http://dx.doi.org/10.1016/j.colsurfa.2013.04.055.

## References

[1] G.J. Vermeij, A Natural History of Shells, Princeton University Press, New Jersey, 1993.
[2] Q. He, Y. Cui, J. Li, Molecular assembly and application of biomimetic microcapsules, Chem. Soc. Rev. 38 (2009) 2292.
[3] T. Boudou, K. Ren, G. Blin, C. Picart, Multiple functionalities of polyelectrolyte multilayer films: new biomedical applications, Adv. Mater. 22 (2010) 441.

[4] M.F. Haase, D.O. Grigoriev, H. Möhwald, D.G. Shchukin, Development of nanoparticle stabilized polymer nanocontainers with high content of the encapsulated active agent and their application in water-borne anticorrosive coatings, Adv. Mater. 24 (2012) 2429.
[5] X. Wang, W. Zhou, J. Cao, W. Liu, S. Zhu, Preparation of core–shell $CaCO_3$ capsules via Pickering emulsion templates, J. Colloid Interface Sci. 372 (2012) 24.
[6] M. Fujiwara, K. Shiokawa, K. Morigaki, Y. Zhu, Y. Nakahara, Calcium carbonate microcapsules encapsulating biomacromolecules, Chem. Eng. J. 137 (2008) 14.
[7] J.A. Thomas, L. Seton, R.J. Davey, C.E. DeWolf, Using a liquid emulsion membrane system for the encapsulation of organic and inorganic substrates within inorganic microcapsules, Chem. Commun. 10 (2002) 1072.
[8] G. Hadiko, Y.S. Han, M. Fuji, M. Takahashi, Synthesis of hollow calcium carbonate particles by the bubble templating method, Mater. Lett. 59 (2005) 2519.
[9] N. Loges, K. Graf, L. Nasdala, W. Tremel, Probing cooperative interactions of tailor-made nucleation surfaces and macromolecules: a bioinspired route to hollow micrometer-sized calcium carbonate particles, Langmuir 22 (2006) 3073.
[10] D. Walsh, B. Lebeau, S. Mann, Morphosynthesis of calcium carbonate (vaterite) microsponges, Adv. Mater. 11 (1999) 324.
[11] Y.S. Han, G. Hadiko, M. Fuji, M. Takahashi, A novel approach to synthesize hollow calcium carbonate particles, Chem. Lett. 34 (2005) 152.
[12] F.C. Meldrum, Calcium carbonate in biomineralisation and biomimetic chemistry, Int. Mater. Rev. 48 (2003) 187.
[13] D.V. Volodkin, N.I. Larionova, G.B. Sukhorukov, Protein encapsulation via porous $CaCO_3$ microparticles templating, Biomacromolecules 5 (2004) 1962.
[14] M. Kitamura, Crystallization and transformation mechanism of calcium carbonate polymorphs and the effect of magnesium ion, J. Colloid Interface Sci. 236 (2001) 318.
[15] X.G. Cheng, P.L. Varona, M.J. Olszta, L.B. Gower, Biomimetic synthesis of calcite films by a polymer-induced liquid-precursor (PILP) process 1. Influence and incorporation of magnesium, J. Cryst. Growth 307 (2007) 395.
[16] Y. Long, B. Vincent, D. York, Z.B. Zhang, J.A. Preece, Organic–inorganic double shell composite microcapsules, Chem. Commun. 46 (2010) 1718.
[17] Z. Zhang, R. Saunders, C.R. Thomas, Mechanical strength of single microcapsules determined by a novel micromanipulation technique, J. Microencapsulation 16 (1999) 117.
[18] A. Kumar, V. Katiyar, Modeling and experimental investigation of melamine-formaldehyde polymerization, Macromolecules 23 (1990) 3729.
[19] I.W. Cheong, J.S. Shin, J.H. Kim, Preparation of monodispersed melamine-formalehyde microspheres via dispersed polycondensation, Macromol. Res. 12 (2004) 225.
[20] M. Okano, Y. Ogata, Kinetics of the condensation of melamine with formaldehyde, J. Am. Chem. Soc. 74 (1952) 5728.
[21] Y. Long, D. York, Z. Zhang, J.A. Preece, Microcapsules with low content of formaldehyde: preparation and characterization, J. Mater. Chem. 19 (2009) 6882.
[22] S. Jahromi, Storage stability of melamine-formaldehyde resin solutions, 1 – the mechanism of instability, Macromol. Chem. Phys. 200 (1999) 2230.
[23] G. Sun, Z. Zhang, Mechanical properties of melamine-formaldehyde microcapsules, J. Microencapsulation 18 (2001) 593.